Two-dimensional infrared spectra reveal relaxation of the nonnucleoside inhibitor TMC278 complexed with HIV-1 reverse transcriptase

Chong Fang[†‡], Joseph D. Bauman[§], Kalyan Das[§], Amanda Remorino[†], Eddy Arnold[§], and Robin M. Hochstrasser[†¶]

[†]Department of Chemistry, University of Pennsylvania, Philadelphia, PA 19104-6323; and [§]Center for Advanced Biotechnology and Medicine and Department of Chemistry and Chemical Biology, Rutgers University, Piscataway, NJ 08854-5638

Contributed by Robin M. Hochstrasser, October 1, 2007 (sent for review September 10, 2007)

The two nitrile groups at the wings of the nonnucleoside HIV-1 reverse transcriptase (RT) inhibitor TMC278 are both identified in high-sensitivity 2D IR spectroscopy experiments of the HIV-1 RT/TMC278 complex. The vibrational spectra indicate that the two arms of the inhibitor sense quite different environments within the hydrophobic pocket. The vibrational relaxation of the two arms are almost equal at 3 ps from model studies. The 2D IR spectra expose a significant distribution of nitrile frequencies that diffuse at equilibrium on ultrafast time scales ranging from hundreds of femtoseconds to tens of picoseconds. The slow spectral diffusion of the cyanovinyl arm of the inhibitor is attributed to its interaction with the backbone and side chains in the hydrophobic tunnel. The results show that the inhibitor cyano modes lose memory of their structural configurations relative to the hydrophobic pocket within tens of picoseconds. The cross-peaks between the two arms of the drug are tentatively attributed to relaxation of the nitrile state with both arms excited.

2D IR spectroscopy | ultrafast protein response | vibrational relaxation

Reverse transcriptase (RT) enables the conversion of a single-stranded RNA into a double-stranded DNA in a process that is essential for viral replication. The nonnucleoside inhibitors of HIV-1 RT (NNRTIs) bind in a hydrophobic pocket between two β-sheets, one containing the polymerase active site and the other containing the *primer grip*, a structural element that is involved in positioning the 3′ primer terminus for catalysis (1). Resistance to NNRTIs can arise from mutations in the residues in and around the binding pocket (2). An NNRTI that has strategic flexibility can overcome the effects of drug-resistance mutations by adapting its conformation and position to accommodate mutation-induced changes in the binding pocket (3). The diarylpyrimidine (DAPY) NNRTI TMC278 (4) is a flexible molecule and inhibits a broad spectrum of NNRTI-resistant mutants. Questions then arise as to freedom of motion of the inhibitor and the time scales of such structural reorganizations. To obtain answers there is a need for time-sensitive probes of structure within the pocket that can respond to motions of the drug and the nearby residues. One set of probes that do not perturb the structure and that span the short time regime are the vibrations of the chemical bonds of the inhibitor. They sense the fluctuations of the surrounding structure through the time correlation functions of their vibrational frequencies. These correlation functions can be measured with the methods of 2D IR spectroscopy (5), and the present work is an application of 2D IR spectroscopy aimed at exposing dynamical aspects of the enzyme inhibitor complex at the chemical bond-length scale. There have been many recent experimental and theoretical advances showing that these methods can expose novel aspects of ultrafast processes in biological assemblies (6–18). The present article on the vibrational spectra and dynamics of an HIV-1 RT inhibitor complex represents a significant challenge to the sensitivity of the 2D IR method.

The x-ray diffraction results (19) provide the essential details of the average structure of the enzyme–inhibitor complex (see Fig. 1) on which interpretations of the nonlinear spectroscopy are based. In the 2D IR experiments the enzyme pocket dynamics are revealed through the fluctuations of the nitrile (–C≡N) vibrational frequencies of the inhibitor. In principle, any type of intermolecular interaction that modifies the vibrational frequency of the probe should show up in the equilibrium dynamics of the probe frequency distribution. The 2D IR echo method not only senses the fluctuating fields created by motions of more distant atoms of the protein but probes any variations of vibrational frequency that arise from dispersion interactions and charges that are *local* to the bound TMC278 molecule.

Reports on the nitrile vibrational mode abound, including work on solvent effects (20), hydrogen bond exchange (21), incorporation into peptides (22), and electric field effects on its spectrum (23–25). The aims of the present work differ from experiments that measure the *time-averaged* electrostatic field effects, such as the recent study of a nitrile inhibitor of human aldose reductase (26). The frequency fluctuations are determined in part by the *time-dependent* electric fields at the nitrile group. It should be noted that the static IR and Raman spectra of polar groups such as nitrile do not reveal the underlying dynamics, because the spectral diffusion seriously invalidates any simple lineshape modeling.

Results

FTIR Spectra. The compounds cinnamonitrile (Ph–C=C–C≡N, A) and benzonitrile (Ph–C≡N, B) were used to model the structures of the two arms of the drug (Fig. 1). Their FTIR spectra in a number of solvents, given as (ν_A, W_A; ν_B, W_B; and R), where ν_A and ν_B (cm^{-1}) are the nitrile stretching frequencies, W_A and W_B (cm^{-1}) are the full widths at half maximum, and R is the ratio of the integrated cross-sections A/B, were as follows: DMSO (2,216, 7.6; 2,228, 7.4; 1.5), acetone (2,220, 5.8; 2,231, 6.3; 2.1), THF (2,219, 5.9; 2,230, 6.6; 1.7), $CHCl_3$ (2,222, 8.8; 2,232, 8.6; 1.6), CCl_4 (2,223, 6.6; 2,233, 7.2; 2.1), and MeOH (2,222, 12; 2,233, 11; 2.1). The cyanovinyl CN group stretching transition is always at lower frequency and has a higher integrated absorption cross-section than that of benzonitrile. The range of the peak separations (ν_B–ν_A) is 10.2–12.2 cm^{-1}, the integrated cross-section ratios (A/B) is 1.5–2.1, and the peak extinction ratios is 1.7–2.3. The transition dipoles of the nitrile transitions in DMSO were 0.087 D for A and 0.071 D for B, comparable to published data (23). Model compounds with amino or alkylamino groups

Author contributions: E.A. and R.M.H. designed research; C.F. performed research; J.D.B., K.D., and E.A. contributed new reagents/analytic tools; C.F., J.D.B., K.D., and A.R. analyzed data; and C.F. and R.M.H. wrote the paper.

The authors declare no conflict of interest.

[‡]Present address: Department of Chemistry, University of California, Berkeley, CA 94720.

[¶]To whom correspondence should be addressed. E-mail: hochstra@sas.upenn.edu.

© 2007 by The National Academy of Sciences of the USA

www.pnas.org/cgi/doi/10.1073/pnas.0709320104

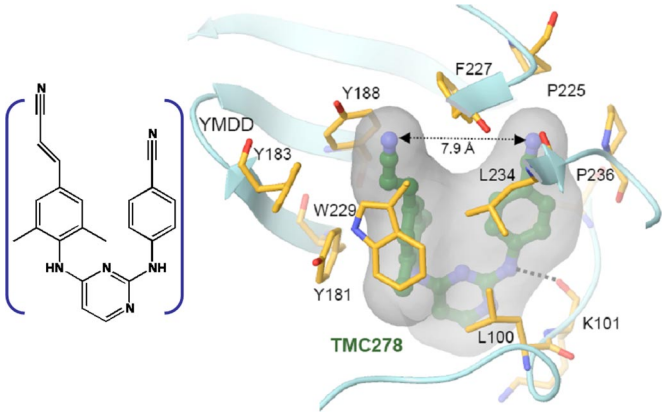

Fig. 1. Structure at 1.8-Å resolution of the HIV-1 reverse transcriptase enzyme RT52A complexed with the NNRTI drug TMC278 (19). (*Left*) The inhibitor. (*Right*) A simplified view of TMC278 in the binding pocket. The dashed line connects the cyanovinyl and benzonitrile CN groups. The cyanovinyl arm extends into a hydrophobic tunnel formed by the side chains of Tyr-181, Tyr-188, Phe-227, Leu-234, and Trp-229.

para to the CN or C=C–CN groups showed the same general trends in their IR spectra.

The HIV-1 RT inhibitor TMC278 (R278474) exhibited a single IR absorption peak in DMSO (2,216 cm^{-1}; W = 9.7), acetone (2,219 cm^{-1}; W = 8.0), THF (2,220 cm^{-1}; W = 8.0), nitrobenzene (2,220 cm^{-1}; W = 9.7), and MeOH (2,225 cm^{-1}; W = 13.6 cm^{-1}), indicating that in all solutions the nitriles at both arms peak at the same frequency within the uncertainty of the bandwidth. However, in the complex the drug displays at least two bands (Fig. 2). The drug binds to RT52A, a recombinant form of HIV-1 RT (J. D. Bauman and E. Arnold, unpublished data), in a 1:1 ratio at millimolar concentrations and its residual concentration was $<\approx 1$ μM. Comparison of the FTIR spectra of RT52A/TMC278 with the spectra of the model compounds suggests an assignment of the nitriles of the complex whose FTIR spectra are shown in Fig. 2. The broad water combination band at 2,130 cm^{-1} dominates the IR absorption in the CN stretch region (Fig. 2*a*). The nitrile spectral region of the complex shows two transitions, one at $\approx$2,214.5 cm^{-1} (W $\approx$ 10 cm^{-1}) and the other at $\approx$2,227.2 cm^{-1} (W $\approx$ 11.5 cm^{-1}). No noticeable changes in the samples of the complex were seen at ambient temperature over a period of 2–6 days. The model compounds show different frequencies for the cyanonitrile and benzonitrile CN transitions, similar to what is observed in the complex, but the drug shows only one band in solvents, so the actual frequency separation between the two arms must be less than found for the models. The ratio of the absorption coefficients of the two bands of the complex (1.6) is the same as found for the models within the concentration uncertainties of the experiments on the drug–protein complex.

2D IR Spectra. The 2D IR results depend on the time intervals of the three-pulse vibrational echo experiment and their frequency transforms: τ and ω_τ, the coherence parameters; T, the waiting time; and t and ω_t, the detection parameters (see *Materials and Methods*). Fig. 3 shows a selection of four of the 2D IR correlation spectra from a total of 25 taken under identical conditions, apart from the changes in waiting time. There are key points to note regarding these results. Each spectrum shows pairs of positive peaks along the diagonals at 2,214 cm^{-1} and 2,227 cm^{-1} and negative peaks shifted along the ω_t axis from these diagonal peaks by ≈ -23.5 cm^{-1}. The lower-frequency diagonal peak signal in 2D IR spectroscopy is $\approx$2.6 times that of the higher-frequency peak signal, which is equal to the square of the

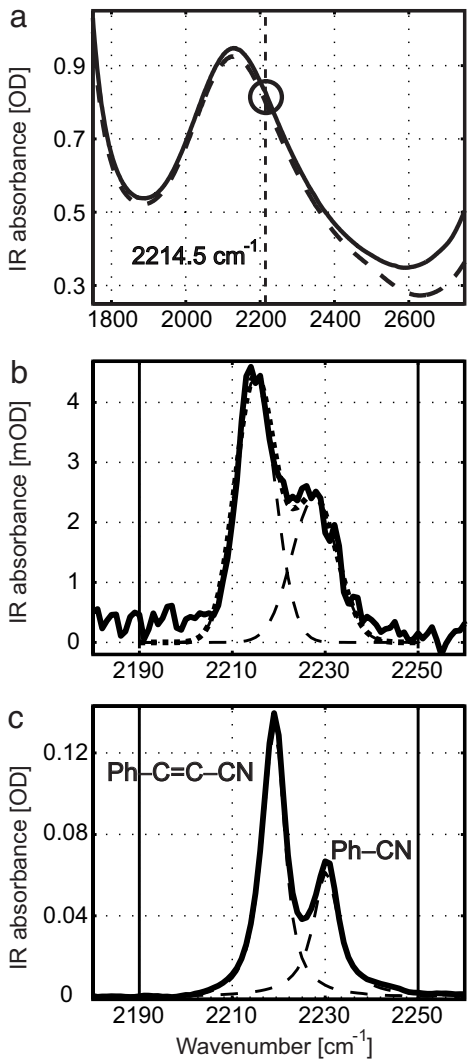

Fig. 2. The FTIR spectrum of the HIV-1 RT/TMC278 complex and model compounds (see *Materials and Methods*). (*a*) The dominant IR absorption from the water (solid line) combination band at 2,130 cm^{-1}. The sample peak region is circled. (*b*) A blowup of the nitrile stretch region of HIV-1 RT/TMC278. The two Gaussian-fitted peaks are shown in dashed lines and their sum in the dotted line. (*c*) The sum of equal molarities of the model compounds benzonitrile and cinnamonitrile in THF with the Voigt profile-fitted curves. The least-squares fitting region is marked by the two vertical solid lines.

ratio found in FTIR. As T progresses, the signals weaken because of population relaxation of the CN vibrations in the range of 3 ps for both arms. A cross-peak at ω_τ = 2,200 cm^{-1}, ω_t = 2,214 cm^{-1} reveals a diagonal peak at 2,200 cm^{-1} that is too weak to be seen directly either in the FTIR or the 2D IR spectrum. This effect occurs (27) because the cross-peak depends on the geometric mean of the coupled-mode intensities. A significant cross-peak also occurs at ω_τ = 2,214.5 cm^{-1}, ω_t = 2,227.2 cm^{-1} linking the two nitrile arms of the drug (Fig. 3). Because of the large contribution from water near T = 0 for the nonrephasing sequence, the complex absorptive spectrum before T = 200 fs is distorted. However, the rephasing sequence contains a greatly diminished water background signal and Fig. 4 shows the magnitude of the rephasing spectrum at earlier waiting times.

Fig. 5 summarizes the evolution of the shape of the 2D IR correlation spectrum from fitting the v = 0 $\rightarrow$ 1 diagonal peak region of the cyanovinyl nitrile stretch to ellipses having major and minor axes a and b at each value of the waiting time. The

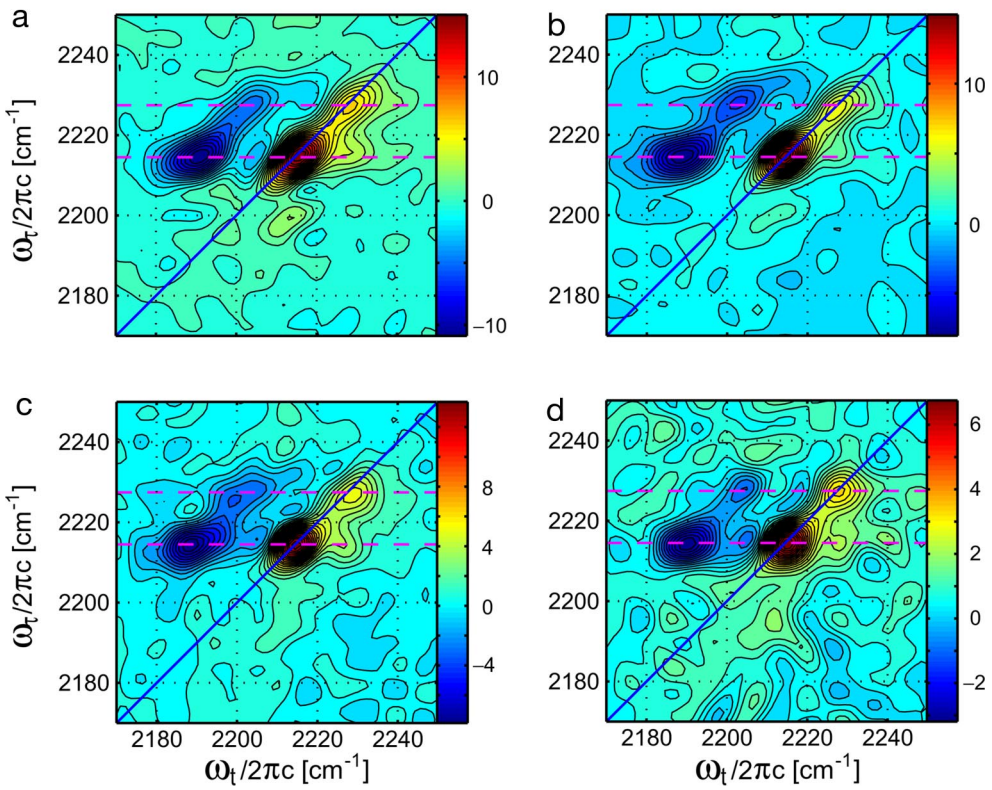

Fig. 3. 2D correlation spectra of the HIV-1 RT/TMC278 complex in aqueous buffer solution with the following waiting times: T = 200 fs (*a*), T = 500 fs (*b*), T = 1 ps (*c*), and T = 3 ps (*d*). The nitrile stretching modes of the two drug wings are indicated by dashed lines at ω_τ = 2,214.5 cm^{-1} and 2,227.2 cm^{-1}, respectively. Positive peaks are red and negative peaks are blue.

ellipses enclosed the spectrum above a certain threshold (see *Materials and Methods*) and the plot is $M(T) = (a^2 - b^2)/(a^2 + b^2)$ vs. T. The solid line is a fit to two exponentials. The dashed line derives from a simulation of the vibrational mode dynamics (see *Materials and Methods*).

Discussion

Both the linear and 2D IR results provide information about the HIV-1 RT/TMC278 pocket. They indicate (Figs. 2–4) the presence of two transitions in the nitrile stretch region, with the stronger one at lower frequency. Assignments of these bands to the two arms of the drug are strongly suggested by the data. The 2D IR results reveal significant heterogeneity in the nitrile frequencies which undergo fast relaxation at the C=C–CN arm of the inhibitor.

The IR spectra in the 2,200 cm^{-1} region are local –C≡N stretching modes. This was verified for the drug TMC278 by computations of its normal modes at the B3LYP/6–31/G** level of theory that found two uncoupled nitrile vibrations, both >97% localized. The lower-frequency mode with the larger cross-section appears to correspond to the –Ph–C=C–CN arm, and the weaker, higher-frequency mode corresponds to the –Ph–CN arm of the drug. Remarkably, the drug exhibits only a single band in all of the solvents but shows two bands in the enzyme pocket. This result immediately suggests that the two nitrile ends of the inhibitor are associated with pocket regions having different polarity or electric fields, corresponding roughly to the difference between DMSO at the –Ph–C=C–CN arm and carbon tetrachloride or methanol at the higher-frequency –Ph–CN arm. The cyanovinyl arm of the drug occupies a hydrophobic tunnel formed by the side chains of Tyr-181, Tyr-188, Phe-227, Leu-234, and Trp-229. Any H-bonded form of this CN group present in the equilibrium distribution would be expected to be up-shifted by ≈8 cm^{-1} from the main cinnamonitrile band (21).

Discussions of dynamics will focus on the stronger mode at ≈2,215 cm^{-1} in 2D IR spectroscopy, which is attributed to cyanovinyl for reasons given above. The diagonal peaks are the v = 0 → 1 transitions of the nitrile stretches, and the peaks displayed in the 2D IR spectra of Fig. 3 that are shifted to lower frequency along the ω_t axis are the v = 1 → 2 transitions. The amount of the shift is the diagonal anharmonicity, which is *ca.* 23 cm^{-1} for both modes. The anharmonic shift is similar to that reported for acetonitrile in ref. 21, which is an additional confirmation of the signal being a nitrile local mode. The 2D spectral shapes and the relative strengths of the diagonal and cross-peaks provide information on the interactions of the vibrators with their surroundings.

The 2D IR spectra report on the frequency fluctuations of the probed CN vibrational modes. The range of structures present in the equilibrium distribution at any instant are manifested as a frequency distribution of the vibrational transitions of inhibitor and RT configurations. Given sufficient time, the complex will visit the complete range of attainable structures causing a relaxation or diffusion of the CN mode frequencies. The spectral diffusion in proteins and peptides have been reported for amide-I bands of the peptide backbone (7, 28) or for ligands such as carbon monoxide in hemoglobin and myoglobin (29–32) and horseradish peroxidase (33) or azide in carbonic anhydrase (29). The time scales for such relaxations are measures of the dynamics of the interchange of protein configurations that may stretch over many decades of time. The ultrafast time scale relaxations usually arise because of the superimposed electric field-induced frequency shifts from the small motions of many charged atoms. Most proteins and organized peptides exhibit a small component of fast spectral diffusion of their vibrations having this origin

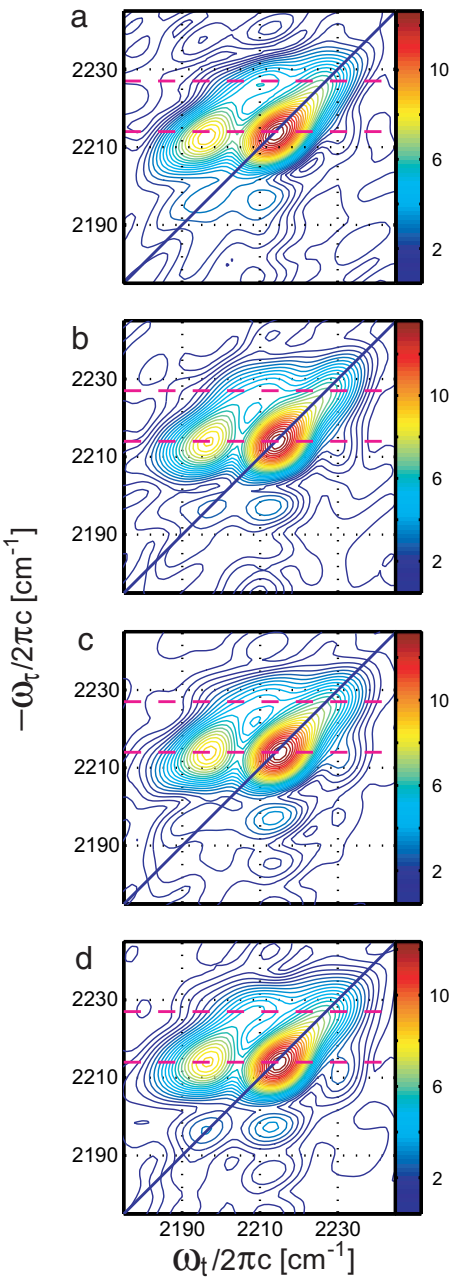

Fig. 4. The rephasing magnitude spectra of the HIV-1 RT/TMC278 complex in aqueous buffer solution at very early waiting times: $T = 0$ fs (*a*), $T = 50$ fs (*b*), $T = 100$ fs (*c*), and $T = 150$ fs (*d*). Two dashed lines at $\omega_\tau = 2{,}214.0$ cm^{-1} and 2,227.0 cm^{-1} indicate the two nitrile stretching modes of the drug. Thirty contour lines are drawn between zero and the peak maximum in each case.

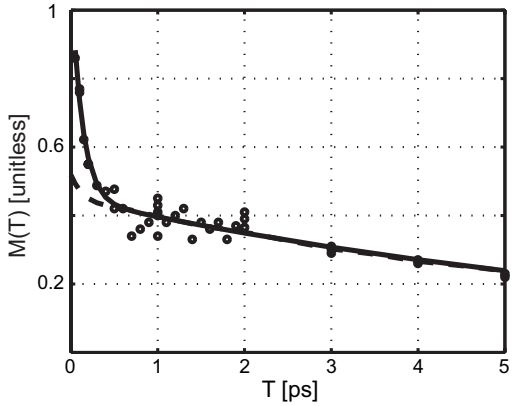

Fig. 5. The ultrafast dynamics of the v = 0 → 1 transition of the cyanovinyl nitrile stretching mode of the HIV-1 RT/TMC278 complex. The elliptical parameter $M(T)$ vs. T plot (circles) is least-squares fitted by a biexponential (solid line), and the simulation is based on quantum-response functions and the set of parameters derived from the experiment (dashed line).

(31). In addition, modes that are involved in hydrogen bonding have been shown to undergo fast spectral diffusion as a result of the making and breaking of these bonds causing fluctuations in the vibrational frequencies (34–37). However, complete relaxation of the distribution of frequencies may stretch out to the microsecond regime when configurations that have nearby vibrational frequencies correspond to structures that cannot interchange without major tertiary and quaternary reorganizations. The local CN mode excitation in a hydrophobic pocket of RT has a range of frequencies determined by the distribution of inhibitor conformations and their locations within the pocket as well as by the distribution of pocket structures to which the inhibitor can bind. The electric field fluctuations from motions of charged RT atoms and protein-associated water molecules can also induce fast spectral diffusion. In effect, the CN mode is acting as a probe of the relative motions of nearby residues and their ability to cause inhibitor conformational changes (29). The situation is analogous to that found for the carbon monoxide ligand in myoglobin or hemoglobin where both fast (hundreds of femtoseconds) and slower (tens of picoseconds) relaxations are seen in ambient-temperature photon echo experiments and simulations. The main part of the slower relaxation is dominated by the distance and angular fluctuations of a nearby histidine residue whose location influences the ligand vibrational frequency (29, 31).

The elongation of the 2D IR spectrum along the diagonal, evident from Figs. 3 and 4, implies that there is a distribution of CN frequencies from the inhomogeneous electric fields of the surrounding charges as well as by van der Waals interactions. The changes in shape of the spectrum as the waiting time increases report on the diffusion of these frequencies representing the relaxation of the structure distribution. At a small waiting time, the shapes of the 2D IR v = 0 → 1 bands resemble ellipses elongated close to the diagonal line, but as T increases to 3 ps the peaks appear to be more circular. The major, a, and minor, b, axes of the ellipse were used to find the factor $M(T)$ defined in *Materials and Methods.* This quantity, which is equal to the vibrational frequency correlation function under certain conditions (38), is not expected to directly mimic the correlation function over the whole range of waiting-time values of our experiment; it is nevertheless a useful way to visualize the dynamics. The change in shape of the 2D IR spectrum from elliptical to circular is already evident by inspection of Fig. 3 (later times) and Fig. 4 (early times). The plot in Fig. 5 indicates that the frequency correlations as represented by $M(T)$ decay on two widely separated time scales: a fast process of 130 fs and a slow one in the range of 7 ps (see *Materials and Methods*). A detailed fitting of these values of $M(T)$ to a full set of quantum response functions for the process (39) containing a frequency correlation function having the form

$$\langle \delta\omega_{10}(T)\delta\omega_{10}(0)\rangle = \Delta_1^2 e^{-T/\tau_1} + \Delta_2^2 e^{-T/\tau_2} \qquad [1]$$

yielded the parameters: $\gamma = \Delta_1^2\tau_1 \approx 0.13$ ps^{-1}; $\Delta_2^2 = 0.42 \pm 0.02$ ps^{-2}; and $\tau_2 = 7.1 \pm 0.3$ ps. The quantity γ is the total homogeneous dephasing rate. It implies a homogeneous linewidth of $\approx$1.4 cm^{-1}. This contribution arises because a portion of the CN frequency fluctuations are fast enough to partially

average the frequency spread of the transitions. The value of Δ_2 determines the width of the slowly relaxing vibrational frequency distribution that elongates the 2D spectra along the diagonal at $T = 0$, and τ_2 is the correlation time associated with this distribution. An extrapolation of the experimental plot of $M(T)$ in Fig. 5 suggests that the nitrile frequency distribution could become completely relaxed on the tens-of-picosecond time scale. This extrapolation implies that a large fraction of the enzyme pocket configurations that can shift the CN mode frequency by measurable amounts have been visited as a result of thermal motions during this period.

A blowup of the hydrophobic tunnel region is shown in Fig. 1. The fast part of the correlation function is likely to have contributions from fluctuations in the electric fields because of the motions of many protein polar groups and the protein–water interface. But the overall decay of the correlation should require relaxation of the local environment of the CN group. The deduced preexponential factor Δ_2 corresponds to a width of the CN vibrational frequency distribution of 7 cm^{-1}. The close contact (3.3 Å; Tyr(OH)$\cdots$(NC)– angle is 102°) of the Tyr-188 hydroxyl oxygen with the nitrogen of the –C=C–CN group is not expected to shift the CN vibrational frequency and this was confirmed by density functional theory (DFT) calculations at the B3LYP/6–31/G** level. The FTIR experiments have shown that the CN frequency of the inhibitor in solution is not sensitive to whether the solvent is acetone, THF, or the aromatic nitrobenzene. Therefore, it is unlikely that thermal fluctuations in the direct-dispersion interactions with the aromatic residues forming the hydrophobic tunnel are responsible for the observed spectral diffusion. Furthermore, we have carried out DFT computations of the effect on vibrational frequency of rotations of the vinyl nitrile plane relative to that of the neighboring phenyl plane at the B3LYP/6–31/G** level. Rotations up to 15° resulted in no significant change (<1 cm^{-1}) in the CN mode frequency. Therefore, although the "jiggling" of the inhibitor (3) in the hydrophobic tunnel may involve such rotations, they are not predicted to make a significant contribution to the spectral diffusion. The localized CN vibration is very unlikely to have its frequency modulated by processes occurring at the other arm or the turn region of the inhibitor (Fig. 1).

A number of examples of spectral diffusion have been given significant theoretical attention. For the OH stretch in water (37, 40, 41) and the aqueous azide anion (9) there are extensive quantum chemical computations of the correlations expected for vibrational frequency vs. electric field that allow strong predictions to be made of the frequency fluctuations from dynamics simulations of the fields. Such computations are not yet available for nitriles. Comparisons of experiments with computations of the electrostatics indicate that the average frequency of the nitrile vibration should increase approximately linearly with the average electric field along the C≡N bond direction in a protein environment (26). However, in these electrostatic estimates the field intensity at a point does not give, in any obvious way, the magnitude of the field fluctuation, which is what is obtained from this work. Nevertheless, the average frequencies of the two arms of the drug in the pocket clearly should be determined in part by the different electrostatic fields at the two cyano groups. Because the cyanovinyl arm is embedded in a hydrophobic tunnel, it is reasonable to guess that the electric field at points in the tunnel can be considerably reduced by screening: qualitative estimates of properties of polarizable media would suggest that the aromatic rings forming the wall have the effect of shielding the interior of the tunnel. Furthermore, the polarizability of aromatics is very anisotropic, so angular and positional fluctuations of these substituted aromatic side chains will cause fluctuations in the electric field at the nitrile group. The lower average frequency of the cyanovinyl end is consistent with its being in an electrostatic field that is lower than that for the higher-frequency benzonitrile arm, according to the predictions based on mean Stark shifts (26). But the spectral shift of 12.7 cm^{-1} between these arms is larger than any of the field variations seen for nitriles in mutants of human aldose reductase (26). Because there is no evidence from the high-resolution diffraction results (19) of any water molecules in the tunnel region and because the tyrosine is very unfavorably oriented for H-bond formation, the slow (tens of picoseconds) relaxation of the vibrational frequency appears to be dominated by motions of the Ph–C=C–C≡N arm with respect to side chains composing the hydrophobic tunnel such as the highly charged oxygen of Tyr-188 and polarizable aromatic groups. Further experiments with mutants and modified inhibitors are needed to clarify this picture and more clearly separate the effects of electric fields from dispersion forces.

The 2D IR spectra exhibit cross-peaks between the two arms that would typically arise if there were some type of coupling between the two CN groups: one nitrile arm appears to be sensing whether or not the other is vibrationally excited. The cross-peak clearly appears in the region $\omega_\tau \approx 2{,}215$ cm^{-1}, $\omega_t \approx 2{,}227$ cm^{-1} of Fig. 3. The coupling is not caused by a direct through-space interaction between the >97% localized –C≡N modes. From the atomic coordinates, the distance (R) between the two CN bonds of the inhibitor is ≈7.95 Å, which would generate a maximum possible coupling magnitude $\mu^2/hcR^3 \approx 0.21$ cm^{-1}, assuming optimally aligned parallel side-by-side transition moments (μ). Such a small interaction leads to an undetectably small cross-peak. The cross-peak is present to *ca.* 50% of its intensity at near-zero waiting time, it then grows to a plateau on the hundreds-of-femtosecond time scale, being fully formed by 2–3 ps (see Figs. 3 and 4). The cross-peak could partially arise from vibrational energy transport between the two CN arms through the inhibitor in a relaxation-assisted process (42). A simple calculation (43) shows that redistribution of the energy of one CN mode throughout the molecule could cause a 61 K temperature rise, but only on a time scale longer or equal to the vibrational relaxation. The signal cannot be solely determined by this effect because the relaxation time is 3 ps. More likely, the cross-peak signal is enhanced because the mode having one quantum of vibrational energy on each arm of the inhibitor decays roughly twice as fast as either arm (44). Simulations of the 2D IR spectra indicate that the lifetime of this doubly excited mode needs to be *ca.* 1 ps to generate the cross-peak strength seen in the experiment. This is close to the value of 1.5 ps expected for deactivation of the doubly excited inhibitor. Perhaps both the double-quantum and relaxation-assisted effects contribute to the cross-peaks and future experiments should be able to distinguish them by lineshape analysis.

Conclusions

Both C≡N arms of the inhibitor TMC278 complexed with HIV-1 RT are clearly seen in the 2D IR spectra, both transitions exhibit a distribution of frequencies and have similar T_1 relaxation times of *ca.* 3 ps. The cyanovinyl and benzonitrile arms are demonstrably in different protein environments. The cyanovinyl arm relaxes its nitrile stretching frequency distribution on the tens of picosecond time scale.

Materials and Methods

Linear-IR Spectroscopy. The FTIR spectra were recorded on a PerkinElmer Spectrum 2000 Explorer with 1.0 cm^{-1} resolution at 295 K in a 56-μm CaF_2 cell (Harrick Scientific).

Samples. The HIV-1 RT52A/TMC278 complex in 10 mM 2-amino-2-hydroxymethyl-1,3-propanediol (Tris) and 75 mM NaCl at pH ≈8.0 was originally prepared in 2.5% DMSO and 1.0% *n*-octyl-β-D-glucopyranoside (BOG) whose molar ratios were reduced by buffer exchange to <≈0.002% in the samples for IR spectroscopy. Samples with 150 mg/ml and 120 mg/ml (≈1 mM) of RT52A

protein (J. D. Bauman and E. Arnold, unpublished data) were used in the experiments. The models were benzonitrile (≥99%, Aldrich, CAS 100-47-0) and cinnamonitrile (97%, predominantly trans, Aldrich, CAS 1885-38-7).

2D IR Spectroscopy. The correlation spectra of HIV-1 RT52A/TMC278 were collected by heterodyned photon echo spectral interferometry by using a 64-element MCT array detector (MCT-12-64; InfraRed Associates), with element separation ≈9.48 nm for 100 groove per mm diffraction grating. The echo in the direction $\vec{k}_{PE} = -\vec{k}_1 + \vec{k}_2 + \vec{k}_3$ was combined with a local oscillator (LO) pulse, also centered at ≈2,220 cm^{-1}, and dispersed and recorded by the array detector/boxcar/computer. The sample cell was purged of H_2O and CO_2. The coherence time interval τ between the first two pulses was scanned in 3-fs steps from −3,600 to 0 (nonrephasing) and 0 to +3,600 fs (rephasing). The pulse $\vec{k}_3$ was delayed from 0 to 5 ps from the second pulse ($\vec{k}_2$ for rephasing, or $\vec{k}_1$ for nonrephasing) to obtain the waiting time (T) dependence. The local oscillator beam was advanced on the pulse $\vec{k}_3$ by 1.5 ps.

Generation of the 2D Correlation Spectrum. The time-domain signal $S(\tau, t; T)$ contains a large contribution from water near zero delay between $\vec{k}_3$ and $\vec{k}_{LO}$, whose intensity peaks at $\tau = 0$ and has the excitation pulse (≈80 fs fwhm) width. A similar τ scan width was observed when detecting the water thermal grating signal at $T = 20$ ps. The nitrile signal persists for many picoseconds (T_1 ≈ 3 ps) so a large fraction of the water signal could be eliminated when only echo data after ≈145 fs were used to obtain the 2D IR rephasing spectra (Fig. 4), and correlation spectra (Fig. 3) by adding up equal weights of the properly phased rephasing and nonrephasing spectra.

Population Relaxation. Heterodyned transient gratings on model compounds in THF, in which T is varied at $\tau = 0$ and the signal integrated from ω_t = 2,180 to 2,260 cm^{-1}, gave population relaxation times (T_1) of the v = 1 states of the nitrile stretching modes as 2.93 ± 0.07 ps for benzonitrile and 3.24 ± 0.07 ps for cinnamonitrile.

Time Dependence of the 2D IR Signal Shape. Contour lines ranging from ≈50% to ≈85% of the correlation spectrum diagonal peak maximum were fitted to ellipses by employing a least-squares fitting algorithm. From the elliptical fitting parameters, we obtained the quantity $M(T) = (a^2 - b^2)/(a^2 + b^2)$. The $M(T)$ curve of the $v = 0 \rightarrow 1$ peak of the cyanovinyl arm fits to a biexponential decay (Fig. 5) with the form of $M(T) = a_1 \cdot \exp(-T/\tau_1) + a_2 \cdot \exp(-T/\tau_2)$ in which $a_1 \approx 0.63$, $\tau_1 \approx 126$ fs, $a_2 \approx 0.45$, and $\tau_2 \approx 7.26$ ps.

The response functions were then computed with a trial correlation function (Eq. **1**) and the simulated 2D correlation spectrum $\underline{S}(\omega_\tau, \omega_t; T)$ was subjected to the same elliptical fitting procedure as the experiment. The computation was also compared with the experimental half-Fourier-transformed spectrum $\tilde{S}(\tau_\tau, \omega_t; T)$ at several T values to obtain an echo peak shift. The magnitudes of the diagonal and antidiagonal widths of the ellipses were used to put constraints on Δ_1^2 and Δ_2^2. At each stage the correlation function reproduced the FTIR spectrum within 5%. The analysis showed that the fast drop in $M(T)$ is influenced by the water-background signal. The magnitude of the factor $M(T)$ at longer waiting times (e.g., $T \geq 1$ ps), where the water background is completely negligible, constrains the inhomogeneous contribution to the correlation function. The homogeneous dephasing rate, $\gamma = \Delta_1^2 \tau_1$ quoted in the text, was better determined than either Δ_1 or τ_1.

ACKNOWLEDGMENTS. We thank Dr. Matt Tucker for help with the computations. This research was supported by National Institutes of Health Grants GM12592 and PO148130 (to R.M.H.) and AI 27690 Merit Award and P01 GM066671 (to E.A.) by using instrumentation from NIH RR01348.

1. Jacobo-Molina A, Ding J, Nanni RG, Clark AD, Jr, Lu X, Tantillo C, Williams RL, Kamer G, Ferris AL, Clark P, *et al.* (1993) *Proc Natl Acad Sci USA* 90:6320–6324.
2. Tantillo C, Ding J, Jacobo-Molina A, Nanni RG, Boyer PL, Hughes SH, Pauwels R, Andries K, Janssen PA, Arnold E (1994) *J Mol Biol* 243:369–387.
3. Das K, Clark AD, Jr, Lewi PJ, Heeres J, de Jonge MR, Koymans LMH, Vinkers HM, Daeyaert F, Ludovici DW, Kukla MJ, *et al.* (2004) *J Med Chem* 47:2550–2560.
4. Janssen PAJ, Lewi PJ, Arnold E, Daeyaert F, de Jonge M, Heeres J, Koymans L, Vinkers M, Guillemont J, Pasquier E, *et al.* (2005) *J Med Chem* 48:1901–1909.
5. Hochstrasser RM (2007) *Proc Natl Acad Sci USA* 104:14190–14196.
6. Zhuang W, Abramavicius D, Mukamel S (2006) *Proc Natl Acad Sci USA* 103:18934–18938.
7. Fang C, Hochstrasser RM (2005) *J Phys Chem B* 109:18652–18663.
8. Lee C, Park K-H, Kim J-A, Hahn S, Cho M (2006) *J Chem Phys* 125:114510/1–114510/11.
9. Li S, Schmidt JR, Piryatinski A, Lawrence CP, Skinner JL (2006) *J Phys Chem B* 110:18933–18938.
10. Kolano C, Helbing J, Kozinski M, Sander W, Hamm P (2006) *Nature* 444:469–472.
11. Fang C, Senes A, Cristian L, DeGrado WF, Hochstrasser RM (2006) *Proc Natl Acad Sci USA* 103:16740–16745.
12. Smith AW, Tokmakoff A (2007) *J Chem Phys* 126:045109/1–045109/11.
13. Krummel AT, Zanni MT (2006) *J Phys Chem B* 110:13991–14000.
14. Zheng J, Fayer MD (2007) *J Am Chem Soc* 129:4328–4335.
15. Kurochkin DV, Naraharisetty SRG, Rubtsov IV (2005) *J Phys Chem A* 109:10799–10802.
16. Larsen OFA, Bodis P, Buma WJ, Hannam JS, Leigh DA, Woutersen S (2005) *Proc Natl Acad Sci USA* 102:13378–13382.
17. Cowan ML, Bruner BD, Huse N, Dwyer JR, Chugh B, Nibbering ETJ, Elsaesser T, Miller RJD (2005) *Nature* 434:199–202.
18. Maekawa H, Toniolo C, Broxterman QB, Ge N-H (2007) *J Phys Chem B* 111:3222–3235.
19. Das K, Bauman JD, Clark AD, Jr, Frenkel YV, Lewi PJ, Shatkin AJ, Hughes SH, Arnold E (2008) *Proc Natl Acad Sci USA* 105:1466–1471.
20. Eaton G, Pena-Nunez AS, Symons MCR, Ferrario M, McDonald IR (1988) *Faraday Discuss Chem Soc* 85:237–253.
21. Kim YS, Hochstrasser RM (2005) *Proc Natl Acad Sci USA* 102:11185–11190.
22. Getahun Z, Huang C-Y, Wang T, De Leon B, DeGrado WF, Gai F (2003) *J Am Chem Soc* 125:405–411.
23. Andrews SS, Boxer SG (2000) *J Phys Chem A* 104:11853–11863.
24. Andrews SS, Boxer SG (2002) *J Phys Chem A* 106:469–477.
25. Reimers JR, Zeng J, Hush NS (1996) *J Phys Chem* 100:1498–1504.
26. Suydam IT, Snow CD, Pande VS, Boxer SG (2006) *Science* 313:200–204.
27. Kim YS, Wang J, Hochstrasser RM (2005) *J Phys Chem B* 109:7511–7521.
28. Hamm P, Lim M, DeGrado WF, Hochstrasser RM (1999) *J Phys Chem A* 103:10049–10053.
29. Lim M, Hamm P, Hochstrasser RM (1998) *Proc Natl Acad Sci USA* 95:15315–15320.
30. Fayer MD (2001) *Annu Rev Phys Chem* 52:315–356.
31. Finkelstein IJ, Goj A, McClain BL, Massari AM, Merchant KA, Loring RF, Fayer MD (2005) *J Phys Chem B* 109:16959–16966.
32. Merchant KA, Noid WG, Akiyama R, Finkelstein IJ, Goun A, McClain BL, Loring RF, Fayer MD (2003) *J Am Chem Soc* 125:13804–13818.
33. Finkelstein IJ, Ishikawa H, Kim S, Massari AM, Fayer MD (2007) *Proc Natl Acad Sci USA* 104:2637–2642.
34. Zanni MT, Asplund MC, Hochstrasser RM (2001) *J Chem Phys* 114:4579–4590.
35. Woutersen S, Pfister R, Hamm P, Mu Y, Kosov DS, Stock G (2002) *J Chem Phys* 117:6833–6840.
36. DeCamp MF, DeFlores L, McCracken JM, Tokmakoff A, Kwac K, Cho M (2005) *J Phys Chem B* 109:11016–11026.
37. Schmidt JR, Corcelli SA, Skinner JL (2004) *J Chem Phys* 121:8887–8896.
38. Lazonder K, Pshenichnikov MS, Wiersma DA (2006) *Opt Lett* 31:3354–3356.
39. Mukamel S (2000) *Annu Rev Phys Chem* 51:691–729.
40. Fecko CJ, Eaves JD, Loparo JJ, Tokmakoff A, Geissler PL (2003) *Science* 301:1698–1702.
41. Asbury JB, Steinel T, Kwak K, Corcelli SA, Lawrence CP, Skinner JL, Fayer MD (2004) *J Chem Phys* 121:12431–12446.
42. Kurochkin DV, Naraharisetty SRG, Rubtsov IV (2007) *Proc Natl Acad Sci USA* 104:14209–14214.
43. Henry ER, Eaton WA, Hochstrasser RM (1986) *Proc Natl Acad Sci USA* 83:8982–8986.
44. Kim YS, Hochstrasser RM (2005) *J Phys Chem B* 109:6884–6891.